Journal of Ceramic Processing Research. Vol. 15, No. 6, pp. 398~402 (2014)

J O U R N A L O F
Ceramic Processing Research

Thermoelectric properties of Sb-doped $Mg_2Si_{1-x}Sn_x$ prepared by mechanical alloying and hot pressing

Sin-Wook You[a], Il-Ho Kim[a]*, Soon-Mok Choi[b] and Won-Seon Seo[c]

[a]*Department of Materials Science and Engineering, Korea National University of Transportation, Chungju, Chungbuk 380-702, Korea*
[b]*School of Energy, Materials and Chemical Engineering, Korea University of Technology and Education, Cheonan, Chungnam 330-708, Korea*
[c]*Energy and Environmental Materials Division, Korea Institute of Ceramic Engineering and Technology, Seoul 153-801, Korea*

Sb-doped $Mg_2Si_{1-x}Sn_x$ solid solutions were prepared by mechanical alloying and hot pressing. The electrical conduction behavior changed from n-type to p-type with increasing Sn content. The electrical conductivity increased with an increase in Sn content at specific temperatures. Sb-doped $Mg_2Si_{1-x}Sn_x$ solid solutions showed n-type conduction, and the carrier concentration was increased by the doped Sb acting as donors. The absolute value of the Seebeck coefficient decreased with increasing temperature. The lowest thermal conductivity of 1.3 W/mK was obtained by Sb doping. $Mg_2Si_{0.7}Sn_{0.3}$: $Sb_{0.01}$ exhibited a maximum ZT of 0.56 at 723 K.

Key words: Thermoelectric, $Mg_2(Si,Sn)$, Solid solution, Mechanical alloying.

Introduction

Intermetallic compounds of Mg_2X (X: Si, Ge, Sn) and their solid solutions have attracted attention as promising thermoelectric materials that can be used for heat recovery and energy conversion applications at 500-850K [1-6]. Mg_2Si, Mg_2Ge, and Mg_2Sn with an antifluorite structure are narrow-band-gap semiconductors, with indirect band gaps of 0.77 eV [7], 0.74 eV [8], and 0.35 eV [9], respectively. A large Seebeck coefficient (α), a high electrical conductivity (σ), and a low thermal conductivity (κ) are necessary to improve the figure of merit ($ZT = \alpha^2\sigma T/\kappa$), where T is temperature on the Kelvin scale. Consequently, thermoelectric materials with a high ZT value should have a low lattice thermal conductivity and high carrier mobility [10].

Among Mg_2Si-Mg_2Sn, Mg_2Si-Mg_2Ge, and Mg_2Sn-Mg_2Ge solid solutions in the Mg_2X systems, $Mg_2Si_{1-x}Sn_x$ is expected to obtain higher ZT because of the greater difference in atomic mass between Si and Sn [11]. The solid solutions between Mg_2Si and Mg_2Sn have reduced thermal conductivity due to the enhanced short wave-length phonon scattering by the introduction of point defect and optimized band structure such as band inversion and splitting [3]. It is very difficult to prepare Mg_2Si-Mg_2Sn solid solutions by melting processes due to the large differences in vapor pressures of the constituent elements, and the small difference between the boiling temperature of Mg (1380 K) and the melting temperature of Mg_2Si (1358 K). Therefore, it is difficult to control the composition, mainly due to the volatilization and oxidation of Mg. Some attempts have been made to dope Mg_2Si-Mg_2Sn solid solutions with additives to control the semiconducting properties. P-type behavior can be produced by doping with Ag or Cu, and n-type by doping with Al or Bi. In this study, Sb-doped Mg_2Si-Mg_2Sn solid solutions were prepared by mechanical alloying and hot pressing as solid-state synthesis routes. The electronic transport properties and thermoelectric properties were examined.

*Corresponding author:
Tel : +82-43-841-5387
Fax: +82-43-841-5380
E-mail: ihkim@ut.ac.kr;

Experimental Procedures

$Mg_2Si_{1-x}Sn_x$: Sb_m ($0.3 \le x \le 0.7$, $m = 0$ or 0.01) solid solutions were synthesized by mechanical alloying (MA) and consolidated by hot pressing (HP). High-purity Mg (99.99%, < 149 μm), Si (99.99%, < 45 μm), Sn (99.999%, < 75 μm), and Sb (99.999%, < 75 μm) were weighed at a stoichiometric ratio and mixed homogeneously. The mixed powders were loaded with hardened steel balls (diameter of 5 mm) into a hardened steel vial in an Ar atmosphere at a weight ratio of 1 : 20. The vial was then loaded into a planetary ball mill (Fritsch, Pulverisette 5) and ball-milled at 300 rpm for 24 h. The synthesized powders were hot-pressed in a cylindrical graphite die with an internal diameter of 10 mm at temperatures ranging from 873 K to 1073 K under a pressure of 70 MPa for 2 h in a vacuum.

The phases and lattice constants of the synthesized solid solutions were analyzed by an X-ray diffractometer (XRD, Bruker D8 Advance) using Cu K_α

radiation (40 kV, 40 mA) and the Rietveld refinement method (Bruker, TOPAS). The diffraction patterns were measured in the θ-2θ mode (10 to 90 ° 2θ) with a step size of 0.02 °, a scan speed of 3 °/min, and a wavelength of 0.15405 nm. The Hall coefficient measurements were performed in a constant magnetic field (1 T) and electric current (50 mA) using the van der Pauw method at room temperature. The sintered bodies were cut to $3 \times 3 \times 10$ mm^3 for measurements of the Seebeck coefficient and electrical conductivity, and cut to 10 mm (diameter) × 1 mm (length) for thermal conductivity measurements. The Seebeck coefficient and electrical conductivity were measured using the temperature differential and four-probe methods, respectively, with ZEM-3 (Ulvac-Riko) equipment in a He atmosphere. The thermal conductivity was estimated from the thermal diffusivity, specific heat, and density measurements using a laser flash TC-9000H (Ulvac-Riko) system in a vacuum. The thermoelectric figure-of-merit was evaluated from 323 K to 823 K.

Results and Discussion

Fig. 1 shows the X-ray diffraction patterns of the Sb-doped $Mg_2Si_{1-x}Sn_x$ powders prepared by mechanical alloying. The patterns of solid solutions correspond to Mg_2Si (ICDD PDF# 00-035-0773) and Mg_2Sn (ICDD PDF# 00-077-0274), with all peaks located between pure Mg_2Si and Mg_2Sn. $Mg_2Si_{1-x}Sn_x$ solid solutions have been successfully prepared by mechanical alloying. Diffraction peaks were gradually shifted to lower angles with an increase in Sn content. Fig. 2 presents the X-ray diffraction patterns of Sb-doped $Mg_2Si_{1-x}Sn_x$ compacts sintered by hot pressing. The solid solution phases remained constant after hot pressing, but in the equilibrium phase diagram of the Mg_2Si-Mg_2Sn pseudobinary system, the $Mg_2Si_{1-x}Sn_x$ has an immiscibility gap between x = 0.4-0.6 [12] or x = 0.2-0.7 [13], and the Sn-rich phase coexists with the Si-rich phase in this composition range. In this study, these two types of phases were observed for x = 0.3-0.7.

Table 1 lists the lattice constants of the $Mg_2Si_{1-x}Sn_x$ solid solutions and electronic transport properties of Sb-doped $Mg_2Si_{1-x}Sn_x$ solid solutions at room temperature. The lattice constants linearly increased from 0.6485 nm to 0.6665 nm with an increase in Sn content. These values were similar to the reported values of Mg_2Si (0.635 nm) [7] and Mg_2Sn (0.677 nm) [11], respectively. As a result, Sn atoms were solved at Si sites. The increase by Sb doping in the lattice constant was small, because the doping concentration was very low, although Sb atoms were substituted for Si or Sn sites. Undoped $Mg_2Si_{1-x}Sn_x$ solid solutions showed n-type conduction for the composition of x = 0.3, but the electrical conduction changed from n-type to p-type at room temperature for $x \geq 0.5$ due to the intrinsic properties of Mg_2Sn. The Sb-doped $Mg_2Si_{1-x}Sn_x$ solid solutions showed n-type conduction, and the carrier concentration of the solid solutions were increased from 7.4×10^{16} cm^{-3} to 8.0×10^{18} cm^{-3} by

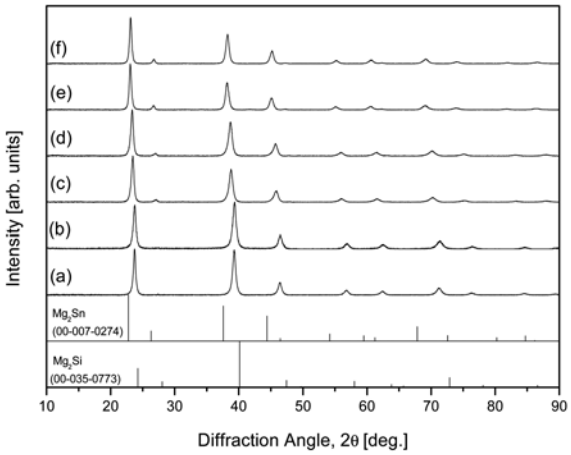

Fig. 1. X-ray diffraction patterns of Sb-doped Mg2Si1-xSnx powders prepared by mechanical alloying; (a) $Mg_2Si_{0.7}Sn_{0.3}$, (b) $Mg_2Si_{0.7}Sn_{0.3}$: $Sb_{0.01}$, (c) $Mg_2Si_{0.5}Sn_{0.5}$, (d) $Mg_2Si_{0.5}Sn_{0.5}$: $Sb_{0.01}$, (e) $Mg_2Si_{0.3}Sn_{0.7}$, and (f) $Mg_2Si_{0.3}Sn_{0.7}$: $Sb_{0.01}$.

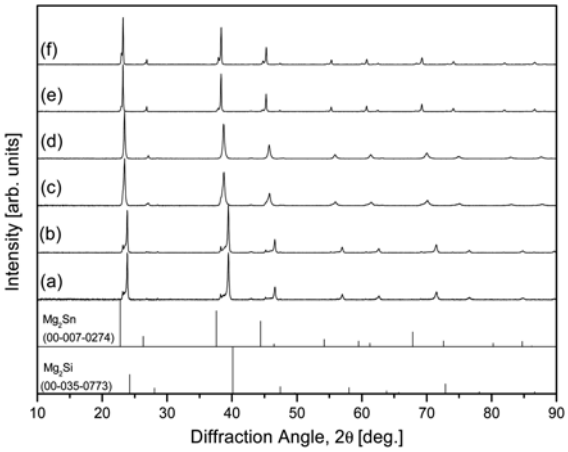

Fig. 2. X-ray diffraction patterns of Sb-doped $Mg_2Si_{1-x}Sn_x$ compacts sintered by hot pressing; (a) $Mg_2Si_{0.7}Sn_{0.3}$, (b) $Mg_2Si_{0.7}Sn_{0.3}$: $Sb_{0.01}$, (c) $Mg_2Si_{0.5}Sn_{0.5}$, (d) $Mg_2Si_{0.5}Sn_{0.5}$: $Sb_{0.01}$, (e) $Mg_2Si_{0.3}Sn_{0.7}$, and (f) $Mg_2Si_{0.3}Sn_{0.7}$: $Sb_{0.01}$.

Table 1. Lattice constants and the electronic transport properties of Sb-doped $Mg_2Si_{1-x}Sn_x$ solid solutions at room temperature.

Specimen	Lattice constant [nm]	Hall coefficient [cm^{3}C^{-1}]	Mobility [cm^{2}V^{-1}s^{-1}]	Carrier concentration [cm^{-3}]
$Mg_2Si_{0.7}Sn_{0.3}$	0.6485	–83.88	30	7.4×10^{16}
$Mg_2Si_{0.7}Sn_{0.3}$: $Sb_{0.01}$	0.6512	–0.78	34	8.0×10^{18}
$Mg_2Si_{0.5}Sn_{0.5}$	0.6562	3.07	3	2.0×10^{18}
$Mg_2Si_{0.5}Sn_{0.5}$: $Sb_{0.01}$	0.6581	–2.26	106	2.8×10^{18}
$Mg_2Si_{0.3}Sn_{0.7}$	0.6665	0.66	7	9.4×10^{18}
$Mg_2Si_{0.3}Sn_{0.7}$: $Sb_{0.01}$	0.6542	–1.49	44	4.2×10^{18}

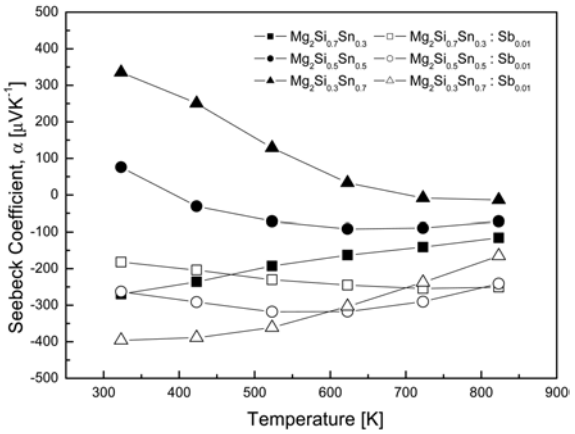

Fig. 3. Temperature dependence of the Seebeck coefficient for Sb-doped $Mg_2Si_{1-x}Sn_x$.

Sb doping. Consequently, Sb atoms worked as n-type dopants (donors) for $Mg_2Si_{1-x}Sn_x$ solid solutions. However, the carrier concentration was decreased by Sb doping for x = 0.7, due to charge compensation by p-type Mg_2Sn.

The Seebeck coefficient (α) of an n-type semiconductor is expressed as Eq. (1) [14, 15]:

$$a=-\frac{k}{e}\left(\frac{5}{2}+r-\frac{E_C-E_F}{kT}\right)=-\frac{k}{e}\left(\frac{5}{2}+r+\ln\frac{N_C}{n}\right)\sim\gamma-\ln n \qquad (1)$$

where k is the Boltzmann constant, e is the electronic charge, r is the exponent of the power function in the energy-dependent relaxation time expression, E_C is the bottom of the conduction band, E_F is the Fermi energy, T is the temperature in Kelvin and N_C is the effective density-of-states in the conduction band, n is the charge carrier concentration and γ is the scattering factor. Fig. 3 presents the temperature dependence of the Seebeck coefficient for Sb-doped $Mg_2Si_{1-x}Sn_x$. In the case of undoped specimens, when x = 0.3, the Seebeck coefficient had a negative sign at all temperatures examined, and for $x \geq 0.5$ the electrical conduction changed from p-type at room temperature to n-type at high temperature. This resulted from the change in the Fermi level and band structure due to the Sn addition. However, for x = 0.7, the Seebeck coefficient had a positive sign at all temperatures examined, while $Mg_2Si_{0.3}Sn_{0.7}$ had a large Seebeck coefficient of 335 μV/K at room temperature, although its carrier density was as high as 9.4×10^{18} cm^{-3}. This could be estimated using both the effects of charge carrier scattering and bipolar conduction due to the formation of a solid solution between Mg_2Si and Mg_2Sn. All Sb-doped specimens showed n-type conduction, and the Seebeck coefficients ranged from −396 μV/K to −164 μV/K.

The electrical conductivity (σ) can be written as [16]:

$$\sigma=\frac{ne^2\tau}{m^*}=ne\mu \qquad (2)$$

where, τ is the relaxation time of the carrier, m* is the effective mass of the carrier and μ is the carrier mobility. The carrier density is related to the reduced Fermi energy by Eq. (3):

$$n=2\left(\frac{2\pi m^* kT}{h^2}\right)^{\frac{3}{2}} exp(\eta) \qquad (3)$$

where $\eta = E_F/kT$ is the reduced Fermi energy. Fig. 4 shows the temperature dependence of the electrical conductivity for Sb-doped $Mg_2Si_{1-x}Sn_x$. In the case of undoped specimens, the electrical conductivity rapidly increased with increasing temperature, indicating non-degenerate semiconducting behavior, and increased with increase in Sn content. The bandgap energies of Mg_2Si and Mg_2Sn were 0.77 eV [7] and 0.35 eV [9], respectively. The electrical conductivity increased because the bandgap energy decreased with increasing Sn content of the sample. For the Sb-doped specimens, the electrical conductivity increased at specific temperature due to an increase in carrier concentration compared to undoped specimens. However, in the case of x = 0.7, the electrical conductivity variation by Sb doping was small, which means that charge compensation occurred, because the majority carriers for Mg_2Sn were holes, and the Sb atoms acted as donors.

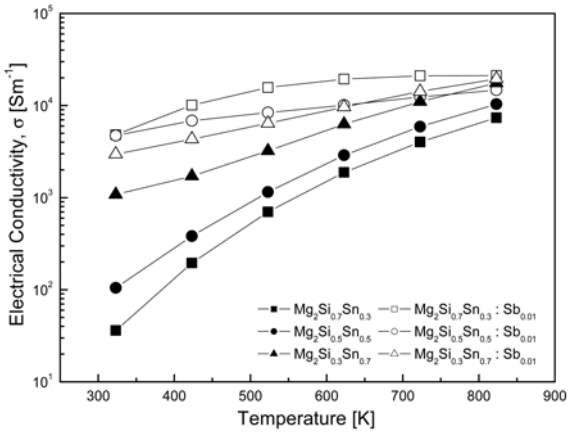

Fig. 4. Temperature dependence of the electrical conductivity for Sb-doped $Mg_2Si_{1-x}Sn_x$.

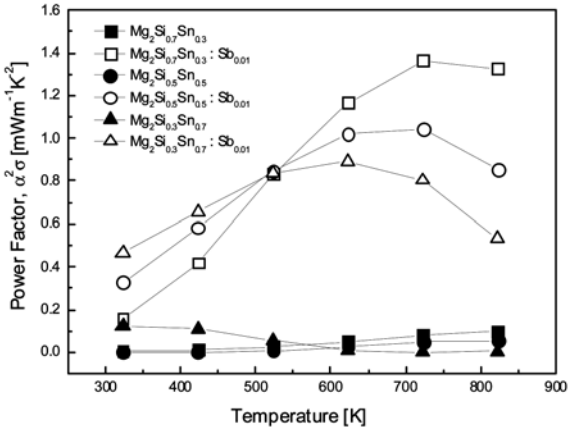

Fig. 5. Temperature dependence of the power factor for Sb-doped $Mg_2Si_{1-x}Sn_x$.

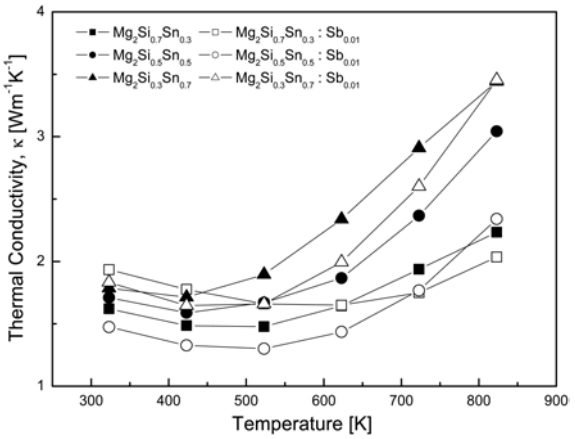

Fig. 6. Temperature dependence of the thermal conductivity for Sb-doped $Mg_2Si_{1-x}Sn_x$.

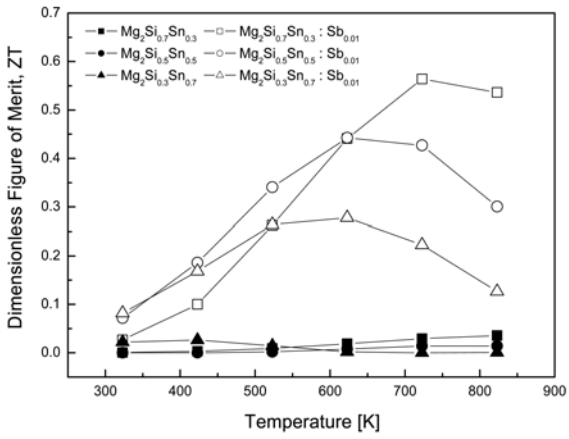

Fig. 7. Temperature dependence of the figure of merit (ZT) for Sb-doped $Mg_2Si_{1-x}Sn_x$.

Fig. 5 presents the temperature dependence of the power factor (PF) for Sb-doped $Mg_2Si_{1-x}Sn_x$. The power factor was calculated by $PF = \alpha^2\sigma$ from the Seebeck coefficient (α) and electrical conductivity (σ). The PF values of undoped specimens were very low, but they were significantly increased by Sb doping. Sb-doped specimens had peak PF values which were decreased with increasing Sn content. The temperature for a peak PF moved to a lower temperature with increasing Sn content. This might be related to the reduction in bandgap energy by Sn addition, which shifted the onset temperature of intrinsic conduction to low temperature.

The thermal conductivity (κ) is the sum of the lattice thermal conductivity (κ_L) due to phonons and the electronic thermal conductivity (κ_E) due to carriers, and it is expressed as [16]:

$$\kappa = dC_pD = \kappa_L + \kappa_E \tag{4}$$

where d is the density, C_p is the specific heat and D is the thermal diffusivity. Both components can be separated using the Wiedemann-Franz law [17]:

$$\kappa_E = \frac{\pi^2}{3}\left(\frac{k}{e}\right)^2 \sigma T = L\sigma T \tag{5}$$

where the Lorenz number is assumed to be a constant ($L = 2.45 \times 10^{-8}\ V^2K^{-2}$) for the evaluation. Fig. 6 indicates the temperature dependence of the thermal conductivity for Sb-doped $Mg_2Si_{1-x}Sn_x$. The thermal conductivity values of Mg_2Si and Mg_2Sn were reported [8] as 6-4 W/mK and 7-3 W/mK at temperatures of 323 K to 823 K, respectively. In this study, Mg_2Si-Mg_2Sn solid solutions exhibited much lower thermal conductivity values of 1.5-3.3 W/mK, which resulted from phonon scattering by a typical alloying effect, where solute (Si or Sn) atoms acted as phonon scattering centers. However, the thermal conductivity of the solid solution increased slightly with an increase in temperature. This could be attributed to an increase in the electronic thermal conductivity due to an increase in the carrier concentration by intrinsic conduction. The thermal conductivity increased with an increase in Sn content at a high temperature, and was slightly reduced by Sb doping due to dopant (ionized impurity) scattering by Sb atoms. The lowest thermal conductivities were 1.3 W/mK for $Mg_2Si_{0.5}Sn_{0.5}$:$Sb_{0.01}$ at 523 K and 1.6 W/mK for $Mg_2Si_{0.7}Sn_{0.3}$: $Sb_{0.01}$ at 623 K.

The dimensionless thermoelectric figure of merit (ZT) that was determined by Eq. (6) [18]:

$$ZT = \frac{\alpha^2\sigma T}{\kappa} \sim \left(\frac{m^*}{m_e}\right)^{3/2} \frac{\mu T^{5/2}}{\kappa_L} \tag{6}$$

where m_e is the mass of an electron. Therefore, a superior thermoelectric material should have a large Seebeck coefficient (large effective mass of carrier), high electrical conductivity (low carrier scattering) and low thermal conductivity (high phonon scattering), simultaneously. Fig. 7 shows the ZT for Sb-doped $Mg_2Si_{1-x}Sn_x$. The ZT values of undoped specimens were very low (below 0.05) at all temperatures examined. However, the ZT was remarkably increased by Sb doping. The maximum ZT value (ZT_{max}) decreased and the peak temperature for ZT_{max} moved to a lower temperature with increasing Sn content. This was related to the reduction in bandgap energy by Sn addition, which shifted the onset temperature of intrinsic conduction to low temperature. In this study, the following was achieved: $ZT_{max} = 0.56$ for $Mg_2Si_{0.7}Sn_{0.3}$: $Sb_{0.01}$ at 723 K, $ZT_{max} = 0.44$ for $Mg_2Si_{0.5}Sn_{0.5}$: $Sb_{0.01}$ at 623 K and $ZT_{max} = 0.27$ for $Mg_2Si_{0.3}Sn_{0.7}$: $Sb_{0.01}$ at 623 K.

Conclusions

$Mg_2Si_{1-x}Sn_x$: Sb_m ($0.3 \le x \le 0.7$, m =0 or 0.01) solid solutions were successfully prepared by mechanical alloying and hot pressing. Sb-doped $Mg_2Si_{1-x}Sn_x$ solid solutions showed n-type conduction, and the carrier concentrations of solid solutions were increased from $7.4 \times 10^{16}\ cm^{-3}$ to $8.0 \times 10^{18}\ cm^{-3}$ by Sb doping. The

electrical conductivity increased with an increase in Sn content, and Sb doping could act effectively to increase carrier concentration and subsequently electrical conductivity. For all specimens, $|\alpha|$ decreased with increasing temperature, and the Seebeck coefficient ranged from $-396\ \mu V/K$ to $-164\ \mu V/K$ for Sb-doped specimens. The thermal conductivity was reduced by the solute atoms that acted as phonon scattering centers. The lowest thermal conductivity of 1.3 W/mK was obtained by Sb doping. $Mg_2Si_{0.7}Sn_{0.3} : Sb_{0.01}$ showed a ZT_{max} value of 0.56 at 723 K.

Acknowledgments

This study was supported by the Fundamental R&D Program for Core Technology of Materials and by the Regional Innovation Center (RIC) Program funded by the Ministry of Trade, Industry and Energy (MOTIE), Republic of Korea.

References

1. V.K. Zaitsev, M.I. Fedorov, E.A. Gurieva, I.S. Eremin, P.P. Kondtantinov, A.Yu. Samunin and M.V. Vedernikov, Phys. Rev. B 74 (2006) 045207.
2. M. Akasaka, T. Iida, K. Nishio and Y. Takanashi, Thin Sol. Film. 515 (2007) 8237.
3. J. Tani and H, Kido, Phys. B 364 (2005) 218.
4. W. Liu, X. Tang and J. Sharp, J. Phys. D: Appl. Phys. 43 (2010) 085406.
5. J. Y. Jung, I. H. Kim, S. M. Choi, W. S. Seo and S. U. Kim, J. Kor. Phys. Soc. 57 (2010) 1005.
6. T. H. An, C. Park, S. M. Choi, W. S. Seo, I. H. Kim and S. U. Kim, J. Kor. Phys. Soc. 60 (2012) 1717.
7. M. Yoshinaga, T. Iida, M. Noda, T. Endo and Y. Takanashi, Thin Sol. Film. 461 (2004) 86.
8. V. K. Zaitsev, M. I. Fedorov, I. S. Eremin and E. A. Gurieva, *Thermoelectrics Handbook*, Ed. D. M. Rowe, Taylor and Francis, (2006) ch. 29.
9. N. Savvides and H.Y. Chen, J. Electron. Mater. 39 (2010) 2136.
10. W. Liu, Q. Zhang, X. Tang, H. Li and J. Sharp, J. Electron. Mater. 40 (2011) 1062.
11. W. Luo, M. Yang, F. Chen, Q. Shen, H. Jiang and L. Zhang, Mater. Sci. Eng. B 157 (2009) 96.
12. S. Wang and N. Mingo, Appl. Phys. Lett. 94 (2009) 203109.
13. Q. Zhang, X.B. Zhao, H. Yin and T.J. Zhu, J. Alloy. Compd. 464 (2008) 9.
14. P. S. Kireev, *Semiconductor Physics*, Mir Publishers, Moscow (1978) p. 253.
15. H. J. Goldsmid, *Electronic Refrigeration*, Pion Limited, London (1985) p. 42.
16. C. Kittel, *Introduction to Solid State Physics*, 6th ed. John Wiely & Sons, Inc. (1986) p. 152.
17. S. W. You and I. H. Kim, Curr. Appl. Phys. 11 (2011) S392.
18. C. B. Vining, *Handbook of Thermoelectrics*, Ed. D. M. Rowe New York, CRC (1995) p. 277.